Available online at www.sciencedirect.com

ScienceDirect

Procedia Structural Integrity 38 (2022) 554–563

Structural Integrity Procedia

www.elsevier.com/locate/procedia

FATIGUE DESIGN 2021, 9th Edition of the International Conference on Fatigue Design

Comparison of the fatigue behavior of wrought and additively manufactured AISI 316L

Tiago Werner[a]*, Mauro Madia[a], Uwe Zerbst[a]

[a]*Bundesanstalt für Materialforschung und -prüfung (BAM), Unter den Eichen 87, 12205 Berlin, Germany*

Abstract

Additive manufacturing (AM) is becoming increasingly important in engineering applications due to the possibility of producing components with a high geometrical complexity allowing for optimized forms with respect to the in-service functionality. Despite the promising potential, AM components are still far from being used in safety-relevant applications, mainly due to a lack of understanding of the feedstock-process-properties-performance relationship. This work aims at providing a full characterization of the fatigue behavior of the additively manufactured AISI 316L austenitic stainless steel and a direct comparison with the fatigue performance of the wrought steel. To this purpose, a set of specimens has been produced by laser powder bed fusion (L-PBF) and subsequently heat treated at 900 °C for 1 hour for complete stress relief, whereas a second set of specimens has been machined out of hot-rolled plates. Low cycle fatigue (LCF) and high cycle fatigue (HCF) tests have been conducted for characterizing the fatigue behavior. The L-PBF material had a higher fatigue limit and better finite life performance compared to wrought material. Both, LCF and HCF-testing revealed an extensive cyclic softening.

Keywords: Additive Manufacturing; L-PBF; 316L; Fatigue; LCF; HCF

* Corresponding author. Tel.: +49 30 8140 3146.
E-mail address: tiago.werner@bam.de

10.1016/j.prostr.2022.03.056

1. Introduction

Additive manufacturing (AM) enables new solutions in design and technology with an almost unlimited freedom with respect to component geometry and the cost-effective production of spare parts. Further potential is in the optimization of structures by customized local geometries and tailored material properties, e.g., at highly stressed regions, the generation of dissimilar material compounds, the incorporation of functional properties, and other items. However, the introduction of this technology for load-bearing components still faces serious difficulties, especially under in-service fatigue loading. These include the reproducibility of properties, both from batch to batch and at different sections across a structure (which causes transferability problems from test specimens to components), a strong tendency to form material defects such as porosity and insufficiently welded regions (lack of fusion), pronounced surface roughness and a complex pattern of high residual stresses in the as-built state.

In view of this problems, Molaei and Fatemi (2019) stated that the "design of critical load carrying parts via AM is still at its infancy because the damage mechanism and evolution of AM metal under cyclic loading are not yet understood." The presence of defects in materials manufactured by a laser powder bed fusion process (L-PBF) makes an application of fracture mechanics interesting for the determination of the fatigue life of L-PBF material and components. Bergant et al. (2021) showed, that approaches based on short-crack propagation models (cyclic R-curve) to L-PBF 316L resulted in good estimates of the experimental data. The cyclic R-curve describes the built up of the fatigue crack-propagation threshold and can be taken as a reference curve for short fatigue crack propagation. It is noteworthy, that the material considered in the study of Bergant et al. (2021) had very large crack initiating defects. They reported effective radii from 60 µm up to 780 µm. A validation of the approach on AM material containing low porosity, closer to the industrial application, is of interest. In view of that, fatigue data and cyclic stress-strain curves are needed.

To provide this information, the present study aims at comparing the fatigue properties of L-PBF and wrought stainless steel 316L. The high cycle fatigue (HCF) properties of these materials were investigated in uniaxial stress-controlled tests and cyclic stress strain curves were obtained using strain-controlled incremental step testing (IST).

Nomenclature

AM	Additive Manufacturing
C	Location parameter in the fitting eq. (1) for HCF-tests according to Basquin (1910)
f	Testing frequency
HCF	High Cycle Fatigue
IST	Incremental Step Test
k	Slope in the fitting eq. (1) for HCF-tests according to Basquin (1910)
LCF	Low Cycle Fatigue
L-PBF	Laser Powder Bed Fusion
N_f	Number of cycles to failure
$N_{90\%}$	Number of cycles at the 90%-probability level of survival
$N_{10\%}$	Number of cycles at the 10%-probability level of survival
R	Load-ratio
$R_{p0.2}$	Yield point with offset 0.2% plastic strain
T_1; ΔT_1	Temperature measured at the grip section of the specimen; difference to initial temperature
T_2; ΔT_2	Temperature measured at the gauge length of the specimen; difference to initial temperature
T_N	Spread of the results in the S-N-diagram $T_N = N_{90\%}/N_{10\%}$, according to DIN50100:2016
ε; $\dot{\varepsilon}$	Applied strain; strain rate
σ; σ_a	Stress; stress-amplitude

2. Factors influencing the fatigue behavior of additively manufactured structures

The local microstructure in metal AM is formed during cooling and temporary reheating of the material volume melted by the laser beam. Since the melt pool is very small, the cooling rate is extremely high (from 10^3 to 10^8 K/s according to Gu et al. (2012)). After a rapid solidification, the material will be reheated when a neighboring track or an additional layer is added. The material is remelted and annealed several times during the building process (Hussain et al. (2013)). Note that the cooling rate is influenced not only by the heat supply, but also by its dissipation. This will change if the bulk temperature gradually increases with time. The properties specific to AM material are the consequence of the thermal history during the manufacturing process:

- **Inhomogeneous and anisotropic Microstructure**, often showing columnar grain-growth through the successive building-layers (e.g. Elangeswaran et al. (2020), Ronneberg et al. (2020)). Cellular structures below grain size are usually reported to be present (e.g. Elangeswaran et al. (2020), Mohr et al. (2020), Ronneberg et al. (2020)). Additional features specific to AM are melt-pool boundaries, which are not necessarily coincident with grain boundaries.
- **Inhomogeneous and anisotropic mechanical properties** as a consequence of the microstructure, both in static (Blinn et al. (2019), Charmi et al. (2021), Ronneberg et al. (2020)) and fatigue loading (e.g. Blinn et al. (2019)). This implies, that the build direction plays a role in the mechanical properties of a component. The term build direction refers to the relationship between building orientation and principal load (or stress) of a component. Note, that this is not always straight-forward in complex shaped AM components.
- **Porosity and surface roughness** have a strong influence on the fatigue properties of AM materials. Typical defects in AM are pores and lack of fusion defects. The latter are usually much more detrimental, because of their big size and their high stress concentration when loaded in building direction. In the as-built state the surface roughness will usually dominate the fatigue behavior (Zhang et al. (2017), Zerbst et al. (2019)).
- **Residual stresses** usually have high magnitudes for laser-based AM techniques in as built condition. Their distribution and magnitude depend on a large variety of factors (e.g. geometry of the component, base-plate heating, time in-between melting of two successive layers). In a vertical built bar, usually a gradient from bottom to top and from outside to the inside is apparent (Zerbst et al. (2021)). The residual stresses in building direction often show the highest magnitudes and are tensile at the surface and compressive in the bulk (e.g. Leutenecker-Twelsiek et al. (2016), Sprengel et al. (2021)). As a result, they are detrimental to the fatigue properties of a component.

Note, that the microstructure and residual stresses are strongly influenced by post-manufacturing treatments. To relieve residual stresses, components are often heat-treated (annealed). For the austenitic stainless steel 316L fabricated by L-PBF studied in the present work, it has been shown, that the microstructure remains stable up to 900°C (Ronneberg et al. (2020), Sprengel et al. (2021)).

3. Material and methods

3.1. Material and specimens

Cuboidal raw bodies have been manufactured using a commercial SLM280 HL system (SLM Solutions Group AG, Germany). The geometry and scanning strategy are indicated in Fig. 1(a). Layers of spherical shaped 316L powder particles with a height of 50 µm were joined using a laser power of 275 W at scanning speeds of 700 mm/s with a hatch distance of 120 µm between neighboring tracks. Mohr et al. (2020) give a more detailed overview on the parameters used. Before removal from the base plate a heat treatment at 450 °C for four hours (HT450) was applied to the raw bodies. Tests on wrought material were performed on hot rolled 316L stainless steel plates. The material was solution annealed at 1100 °C and quenched in water.

Sprengel et al. (2021) showed, that the residual stresses in the building direction of the L-PBF material (HT450) were of magnitudes around 500 MPa towards the surfaces balanced by compressive residual stresses of around -200 MPa at the center of the as-built geometry. To avoid influences of residual stresses, the AM specimens in the current

work have therefore been heat-treated in vacuum at a temperature of 900°C for one hour and subsequently rapidly cooled in argon (HT900). This led to a full stress relieve (Sprengel et al. (2021)).

The grain structure in the material is observed in electron back-scatter diffraction (EBSD) images (Fig. 1(b)): columnar, cup shaped grains and thin, elongated grains between them are present in the L-PBF material. As Sprengel et al. (2021) state, the additional heat treatment keeps the columnar grain structure observed in the condition heat treated at 450 °C, while grain-growth was apparent. They saw that the cellular structure on sub-grain level present in L-PBF material disappeared in the condition HT900. These structures consist of a high density of dislocations and segregated elements due to the rapid cooling. The wrought material investigated showed a globular grain structure (Fig. 1(b)).

L-PBF material in condition HT450 had a yield strength of $R_{p0.2}$ = 500 MPa (Charmi et al. (2020)), while the wrought material is reported to have a yield-strength of $R_{p0.2}$ = 250 MPa by the manufacturer. Tensile tests on L-PBF material in condition HT900 resulted in a value of $R_{p0.2}$ = 388 MPa. This decrease after the heat treatment is in accordance to results published by Ronneberg et al. (2020). An overview on the different material conditions tested is given in Tab. 1.

Round fatigue specimens according to Fig. 1(c) were manufactured from the cuboidal raw bodies. Note that the loading direction is in the building direction. The specimens made from wrought material were oriented in the rolling direction of the material. They had the same geometry as indicated in Fig. 1(c), but longer heads, leading to an overall length of 130 mm.

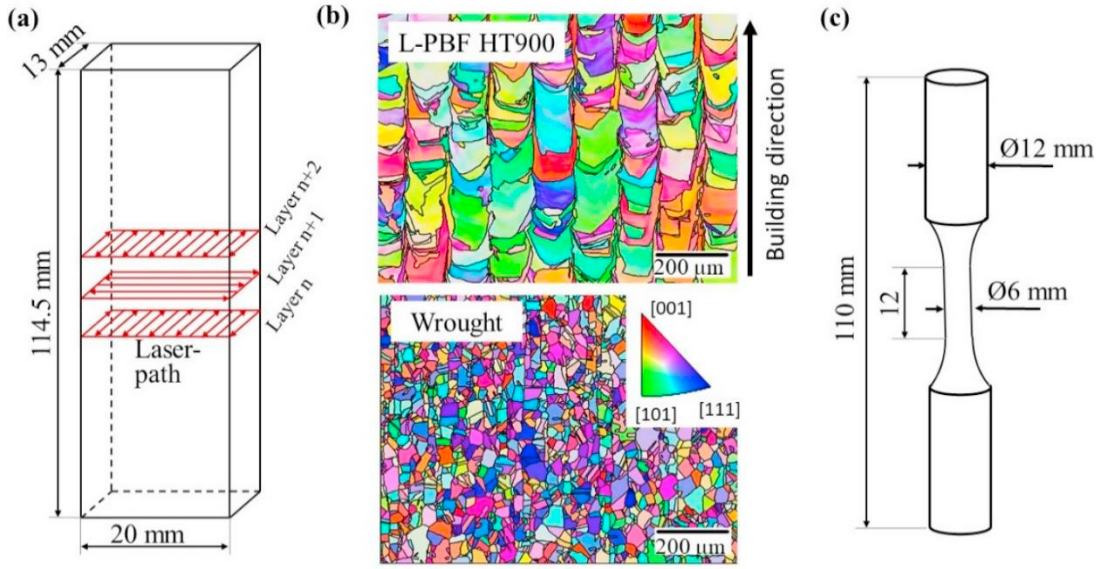

Fig. 1. (a) Schematic representation of a cuboid manufactured by L-PBF for specimen production, including the scanning strategy used; (b) EBSD-images of the microstructure for L-PBF material and wrought material (edited from Sprengel et al. (2021)). The grain orientation is indicated in building direction; (c) Specimen geometry used for HCF and IST testing.

Table 1. Material conditions used for testing.

	Heat-treatment	Cooling	$R_{p0.2}$ (MPa)
Wrought 316L (hot-rolled)	annealed at 1100 °C	quenched in water	250
L-PBF 316L HT450	450 °C for 4h (argon)	furnace cooled	500
L-PBF 316L HT900	HT450 + 900 °C (1 h, vacuum)	rapid cooling in argon	388

3.2. Fatigue testing

To compare the fatigue behavior of wrought and L-PBF material, load controlled tests in the high cycle fatigue regime and strain-controlled tests with variable amplitudes were performed. To this purpose, a servo-hydraulic uniaxial machine with a nominal load of 25 kN (Carl Schenck AG) was used. The hydraulic grips of the machine were aligned before testing to avoid bending loads. For strain-controlled testing, a strain gage extensometer (Instron GmbH) was used to measure the applied strain in the gauge length of the specimen.

The round specimens were electro-chemically polished to a depth of approximately 150 µm to remove surface residual stresses due to grinding using a commercial polishing bath (Arno Graul GmbH). The electrolyte (consisting of phosphoric and sulphuric acid) suitable for stainless steels was provided by the manufacturer of the bath. Subsequent mechanical polishing was applied, to remove irregularities remaining from the electro-polishing process. The roughness of the surface was $R_Z < 0.2$ µm.

3.2.1. Incremental Step Testing

The incremental step test (IST) as described by Christ (1990) was used to obtain the cyclic stress strain curve (CSSC) for the material conditions wrought, L-PBF HT450, L-PBF HT900. The testing procedure consists of a stepwise, linear increase of the applied total strain amplitude and subsequent decrease as shown in Fig. 2(a). These blocks were repeated until failure of the specimen. The stress-response of the material leads to a spiral in the stress-strain-diagram (Fig. 2(b)). The corner points of the spiral describe the CSSC. Metallic materials usually reach a stabilized state, at which the CSSC does not change from block to block. In the present work, the strain-rate was kept constant at $\dot{\varepsilon} = 0.02$ %/s during the test. A minimum amplitude of $\varepsilon = 0.15$ % and a maximum amplitude of $\varepsilon = 0.8$ % were used. The starting block consisted of a decreasing half of a block starting with the maximum strain amplitude. This allows to obtain a quasi-static stress-strain-curve.

Note, that while the IST is not suited for the precise determination of the CSSC obtained by a single step test (Pickard and Knott (1988)), it yields good results for variable amplitude loading scenarios (e.g. Polák et al (1977)). For comparing the cyclic response of the different material conditions (Tab. 1) it is a suited tool.

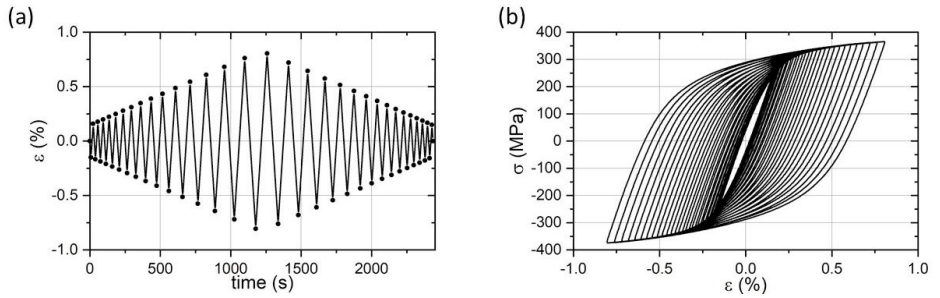

Fig. 2. Incremental Step Test (IST). (a) Strain versus time in one loading-block used in the current work; (b) Exemplary response of the L-PBF HT900 material to the applied strain for one block.

3.2.2. High Cycle Fatigue

HCF-testing was performed on wrought and L-PBF 316L in condition HT900 at alternating loads (load ratio $R = -1$). The specimens were tested up to failure or up to 10^7 cycles, whichever occurred first. The temperature was measured at the top head of the specimens (grip section). This temperature is an indirect indication of heating in the gauge-length due to plastic deformation. During testing of wrought 316L stainless steel specimens considerable heating was observed, depending on load and frequency. To measure the heating in the gauge length of the specimen and refer it to the temperature measured at the head, one wrought specimen was tested with an additional thermocouple at the center of the gauge section. Fig. 3(a) shows the resulting increases in temperature at constant stress amplitude $\sigma_a = 230$ MPa dependent on the frequency applied. The frequency was kept constant, until a stable temperature was reached. A temperature-change of 105 °C from the initial ambient temperature of 26.3 °C was reached in the gauge

length of the specimen at $f = 9$ Hz. A nearly linear relationship between the two measured temperatures was observed. Note, that the amplitude was below the yield strength $R_{p0.2} = 250$ MPa provided by the manufacturer. Even at this stress level, the amount of irreversible mechanisms (plastic deformation) is sufficient to produce a noticeable self-heating of the specimen. For further HCF-testing only the temperature T_1 at the head of the specimen was available. To reduce the heating of the specimen, the increase of this temperature was monitored. If an increase above $\Delta T_1 = 3$ K was seen, the frequency was decreased. Depending on the load applied, this procedure yielded testing frequencies ranging from $f = 0.5$ Hz to $f = 16$ Hz. For the HCF tests already performed on wrought 316L, a maximum temperature in the gauge length of $T_2 = 53.7$ °C was reconstructed using a spare specimen tested at the applied loads and frequencies including a temperature measurement in the gauge length.

4. Results and discussion

4.1. High cycle fatigue

The resulting S-N-diagrams for wrought and L-PBF HT900 material are shown in Fig. 3(b). For wrought 316L, two runouts were observed at $\sigma_a = 210$ MPa. At a stress-level of $\sigma_a = 220$ MPa, two specimens showed number of cycles to failure below 10^6. While for the tests performed a clear fatigue limit and its statistical distribution cannot be extracted, it is suspected to be in the region between 210 MPa and 220 MPa, considering specimens with number of cycles to failure above 10^7 to be loaded below their fatigue limit.

The experimental data were fitted according to the equation proposed by Basquin (1910),

$$N_f = C \cdot \sigma_A^{-k}, \tag{1}$$

with the location parameter $C = 2.16 \cdot 10^{34}$ and the slope $k = 12.266$. All tests above $\sigma_a = 210$ MPa had to be performed at frequencies at or below 4 Hz to avoid self-heating of the specimen. For comparison, data of Huang et al. (2015) on wrought 316L is presented. Their material was solution annealed at 1100 °C for one hour and water quenched as the material in the present work. The yield strength was reported $R_{p0.2} = 205$ MPa. Note, that this is about 20 % lower compared to the value for the material used in the present work. The different plastic properties might explain the difference in the finite life branch and fatigue limit. Additionally, the roughness of the specimens in the work of Huang et al. (2015) is not clear. On the other hand, it is noteworthy that the frequency applied by Huang et al. was 5 Hz for all load levels. It should be therefore expected that a considerable amount of self-heating was generated, which could have influenced the results. This should be even more pronounced, as the lower yield strength suggests larger plastic deformation, given the same applied stress.

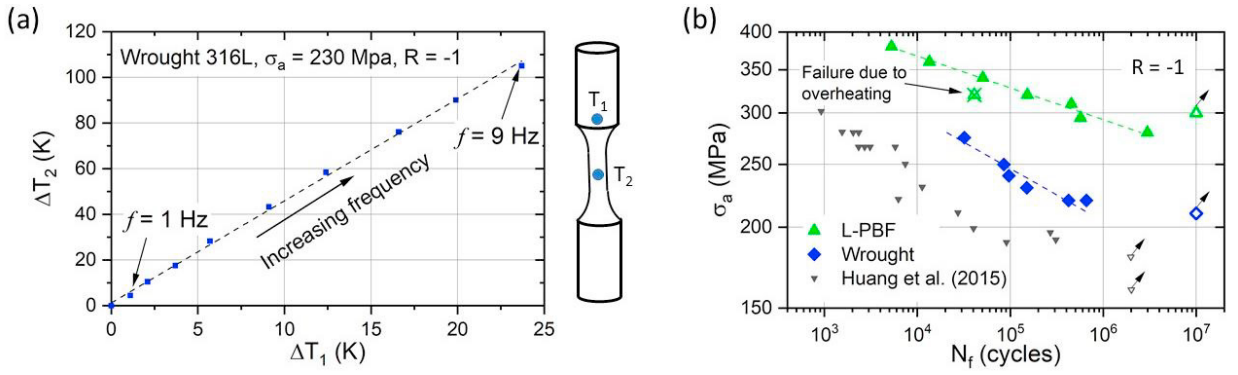

Fig. 3. HCF-testing: (a) Change in temperature dependent on the frequency applied during testing of a specimen (wrought 316L) with respect to ambient temperature; (b) S-N-curves for wrought and L-PBF 316L HT900 including the fit according to eq. (1). Additional data from Huang et al. (2015) for wrought 316L are reported for comparison.

The L-PBF-material was subjected to much higher loads during HCF-testing compared to the wrought material. A distance of two decades between the number of cycles to failure is apparent at the lowest and the highest load applied for L-PBF and wrought 316L, respectively. At σ_a = 300 MPa one runout occurred, while at the lower load of σ_a = 280 MPa the specimen failed after approximately $3 \cdot 10^6$ cycles. While the tests performed do not allow the extraction of the fatigue limit, it is suspected to be in a region between σ_a = 300 MPa and σ_a = 260 MPa. Note that this is 40 MPa to 90 MPa higher compared to the value reached in wrought material. Besides the runout, no big scatter is apparent. A scatter-parameter of $T_N = N_{90\%}/N_{10\%} = 2.13$ was calculated for the datapoints according to DIN50100:2016 compared to T_N = 2.87 for the wrought material. The slope of the S-N-curve is lower for the L-PBF material (parameters for eq. (1): $C = 1.89 \cdot 10^{56}$, $k = 20{,}38$). In contrast to that finding, it would be expected, that the defect-prone L-PBF material would show a steeper slope compared to wrought material. As reported by Blinn et al. (2019), materials are usually more sensitive to defects at low stresses. The finding of the contrary behavior is remarkable. An example for a pore at the crack-initiation-site is shown in Fig. 4. It has a diameter of approximately 30 µm. Note, that the number of cycles to failure for this specimen is not far off the interpolation-line for L-PBF material (Fig. 3). The little scatter observed speaks in favor of similar crack-initiating defects in all specimens, which lead to a low number of cycles to initiate a fatigue crack, implying, that the fatigue crack-propagation behavior of the material controls the number of cycles to failure.

A reason for the reduced slope can be the pronounced softening behavior seen for L-PBF-material at higher loads. Fig. 5(b) shows the difference in displacement of the cylinder of the testing-machine from minimum load to maximum load during the fatigue testing for various loads. For all loads it continuously increases with the number of cycles applied to the specimen. This softening behavior becomes more pronounced with higher loads. In contrast to that, wrought 316L showed a hardening behavior after an initial phase of softening (Fig. 5(c)). Pronounced cyclic softening at higher applied loads decreases the fatigue resistance due to the increasing plasticity in the test. It therefore leads to smaller N_f, which provides an explanation for the less steep S-N-curve, as at low loads softening is less pronounced.

The higher fatigue limit and load amplitudes in the finite life-branch for the L-PBF material compared to the wrought material correlate with its higher yield strength. At an applied amplitude of σ_a = 295 MPa almost no softening is apparent for L-PBF-material in Fig. 5(b), which implies very little plasticity throughout the test (the yield strength of the material is $R_{p0.2}$ = 388 MPa; see Tab. 1). At this load, the wrought material would have experienced massive yielding ($R_{p0.2}$ = 250MPa; see Tab. 1). Given the same applied stress-level, the wrought material would experience a higher plastic deformation, which explains the lower number of cycles to failure at the same load-level compared to the L-PBF material. Due to the load-ratio R = -1, plastic deformation was present throughout the test (inverse plasticity), which is supported by the self-heat generation present in both L-PBF and wrought 316L at the high load-amplitudes resulting in increased temperatures when applying higher testing frequencies.

The increase in plastic deformation due to softening in case of the L-PBF material leads to an increase in the heat produced during the fatigue test. Fig. 5(a) shows a specimen after testing, for which the frequency was not decreased as the temperature increased. The temperature at the specimen's head initially increased and subsequently stayed stable for about 15 min. After this period the temperature continuously increased up to 68 °C. This indicates very high temperatures in the gauge length of the specimen, which is visible in the annealing color in Fig. 5(a). As the temperature increased, the plastic deformation increased and finally the specimen deformed in tension showing necking behavior. The specimen is marked in Fig. 3(b) ("Failure due to overheating").

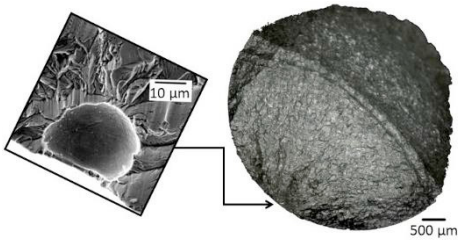

Fig. 4. Fracture surface of the L-PBF-specimen tested at σ_a = 320 MPa. Optical microscopy image for overview, scanning electron microscopy image in secondary electron detector mode for detail image of pore.

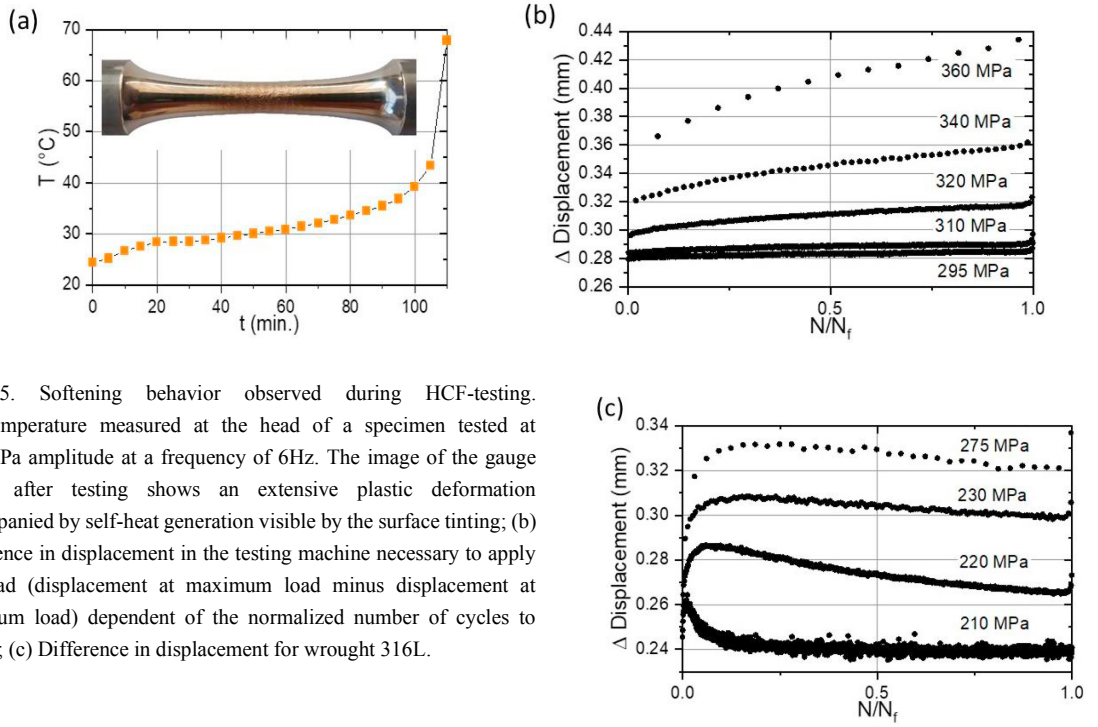

Fig. 5. Softening behavior observed during HCF-testing. (a) Temperature measured at the head of a specimen tested at 320 MPa amplitude at a frequency of 6Hz. The image of the gauge length after testing shows an extensive plastic deformation accompanied by self-heat generation visible by the surface tinting; (b) Difference in displacement in the testing machine necessary to apply the load (displacement at maximum load minus displacement at minimum load) dependent of the normalized number of cycles to failure; (c) Difference in displacement for wrought 316L.

4.2. Incremental Step Testing

Fig. 6 shows results from the IST performed on L-PBF material and wrought material. In addition to the condition HT900, one test was performed on a specimen in condition HT450. The higher yield strength of the L-PBF material in the latter condition is indicated by the higher stress observed at the first maximum strain amplitude (Fig. 6(a)). In both heat-treatment conditions, the L-PBF material shows clear, degressive cyclic softening. A stable state seems to be almost reached around block number 250, even though specimen fracture prevented the observation of a constant line in the diagram. At this point, the maximum stress decreased by 105 MPa and 55 MPa for HT450 and HT900, respectively. Note, that in condition HT900 an initial cyclic hardening from the first to the second block was present, while in condition HT450 cyclic softening was observed from the first block on. In contrast to the softening behavior present in the L-PBF material, the specimen made of wrought 316L displayed extensive hardening in the first block and continuous hardening from block 2 on up to block 300. Subsequently the progressively decreasing stress-amplitude indicates the failure of the specimen. An explanation for the softening behavior in L-PBF 316L is the initially high density of dislocations due to the manufacturing process. As Ronneberg et al. (2020) explain, their reduction leads to a lower yield-strength after a heat-treatment. While the decrease in yield strength indicates a partial dissolution of dislocations due to the heat-treatment HT900, the cyclic softening present in the material is potentially explained by further change in dislocation structure. Note that Ronneberg et al. (2020) provide additional mechanisms for the decrease in yield strength: (i) atomic diffusion dissolving chemical segregations as present in the cellular sub-structures; (ii) change in grain-size, as grain-boundaries provide significant strengthening to the material. These two mechanisms cannot explain the softening during the cyclic experiments, because they need elevated temperatures (as present during heat-treatments).

An explanation for the continuous cyclic hardening of wrought 316L might be the development of martensite due to the plastic deformation during the IST. Bayerlein et al. (1987) showed, that deformation induced martensitic transformation was the reason for this behavior in IST of stainless steel 304L. Martensite is progressively formed during the cyclic deformation, which explains the continuous increase in stress-amplitudes in the IST. As a

quantification of the susceptibility of steels to deformation induced martensitic transformation, the M_{d30}-temperature is the temperature, at which applying 30% of plastic strain 50% of the austenite have transformed to martensite. Angel (1954) found an empirical equation relating M_{d30} to the chemical composition. Table 2 shows the chemical composition of the wrought 316L used in the present work and the composition of 304L stainless steel as investigated by Bayerlein et al. (1987), including the resulting M_{d30}. For the present wrought 316L it is well in the region of 304L, which supports the assumption of cyclic hardening due to martensitic transformation.

To obtain the CSSC shown in Fig. 6(b), a "stabilized" block was chosen from Fig. 6(a). Since no clear plateau is visible for neither of the materials tested, the stabilized maximum loads were chosen to be close to the minimum slope in Fig. 6(a) for L-PBF material – around block 250 – and for wrought material the maximum load was chosen. This was then used, to determine the loading-block at which the maximum load decreased 10 %. The CSSC was taken from the block with half its number. Due to the rapid decrease in maximum load when the specimen starts failing, the CSSC obtained is not sensitive to slight changes in the choice of the stable maximum load. The cyclic behavior was almost symmetric concerning positive and negative loading. For better display, only the positive branches are shown in Fig. 6(b). Note the good agreement between the curves obtained for L-PBF material in condition HT900 compared to wrought 316L.

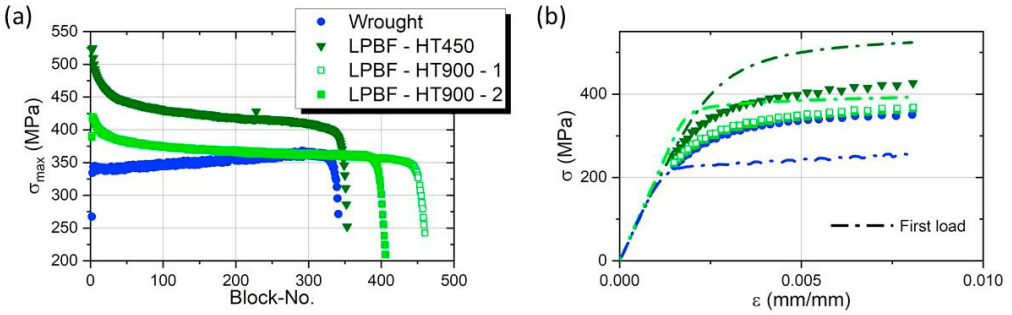

Fig. 6. Results of the IST. (a) Stress at the maximum strain-amplitude of each loading-block; (b) Positive branch of the CSSC extracted at half of block-number, at which the max. stress decreased 10 % from stabilized value. Additionally, the stress-strain-curves corresponding to the first loading are displayed.

Table 2. Chemical composition of the wrought 316L material in weight-% according to the manufacturer and composition range for 304L stainless steel (all Elements but Cr and Ni put to medium value). Includes the M_{d30}-Temperature according to Angel (1954).

Material	C	Si	Mn	P	S	Cr	Ni	Mo	N	Fe	M_{d30} (°C)
304L	0.015	0.5	1.0	0.045	0.015	18 – 20	10 – 12	0.0	0.05	Bal.	-17.7 – 28.7
316L	0.017	0.46	1.23	0.031	0.001	16.9	10.1	2.03	0.05	Bal.	2.8

5. Conclusions

For the present work, stainless steel 316L manufactured by L-PBF was investigated in stress-controlled HCF-testing to obtain an S-N-curve and strain-controlled IST testing to obtain the cyclic deformation behavior of the material. The results are compared to the behavior of wrought material and can be summarized as follows:

- Both wrought and L-PBF 316L, experienced heating due to plastic deformation in the gauge length of the specimens during HCF testing. High temperatures were avoided by reducing the loading frequency. Due to the softening behavior of the L-PBF material, a continuous increase in heat-production could be observed when a specimen was tested at constant load-frequency.
- The L-PBF material withstands higher stress amplitudes compared to the wrought material. This is attributed to the higher yield strength going along with lower plastic deformation at the same load-level. A low scatter is apparent for the L-PBF material, implying, that defects of similar sizes and positions lead to fast crack-initiation and subsequent crack-growth.

- A pronounced cyclic softening was observed for the L-PBF material, both in HCF- and LCF-testing. It was attributed to changes in dislocation structure. Due to rapid, repeated heating and cooling during the production, a high dislocation density is present in L-PBF material, partially decreased by subsequent heat-treatments.

Microstructural analysis on the tested specimens, both in HCF and LCF regime, is in progress to investigate the correlation between cyclic behavior and dislocation movement.

Acknowledgements

This work has been funded by the BAM focus area materials project AGIL "Microstructure Development in Additively Manufactured Metallic Components: from Powder to Mechanical Failure". We are thankful for the financial support and the fruitful cooperation with all partners.

References

Angel, T., 1954. Formation of Martensite in Austenitic Steels, Effects of Deformation, Temperature, and Composition, Journal of the Iron and Steel Institute 177, 165-174.

Bayerlein, M., Christ, H.-J., Mughrabi, H., 1987. A Critical Evaluation of the Incremental Step Test. In: Rie KT. (eds) Low Cycle Fatigue and Elasto-Plastic Behaviour of Materials. Springer, Dordrecht.

Basquin, O.H., 1910. The exponential law of endurance tests, Proc. ASTM 10, 625–630.

Bergant, M., Werner, T., Madia, M., Yawny, A., Zerbst, U., 2021. Short crack propagation analysis and fatigue strength assessment of additively manufactured materials: an application to AISI 316L. Int J Fat, accepted Manuscript.

Blinn, B., Ley, M., Buschhorn, N., Teutsch, R., Beck, T., 2019. Investigation of the anisotropic fatigue behavior of additively manufactured structures made of AISI 316L with short-time procedures PhyBaLLIT and PhyBaLCHT. Int. J. Fat. 124, 389-399.

Charmi, A., Falkenberg, R., Ávila, L., Mohr, G., Sommer, K., Ulbricht, A., Sprengel, M., Saliwan Neumann, R., Skrotzki, B., Evans, A. Mechanical anisotropy of additively manufactured stainless steel 316L: An experimental and numerical study. Mat. Sci. Eng. A 799.

Christ, H.-J., 1991. Wechselverformung von Metallen. Werkstoff-Forschung und -Technik, Springer-Verlag.

DIN50100:2016 Load controlled fatigue testing – Execution and evaluation of cyclic tests at constant load amplitudes on metallic specimens and components.

Elangeswaran, C., Cutolo, A., Muralidharan, G.K., Vynmeensel, K., Van Hooreweder, B., 2020. Microstructural analysis and fatigue crack initiation modelling of additively manufactured 316L after different heat treatments. Materials and Design 194.

Gu, D., Hagedorn, Y.-C., Meiners, W., Meng, G., Batista, R.J.S., Wissenbach, K., Poprawe, R., 2012. Densification behavior, microstructure evolution, and wear performance of selective laser melting processed commercially pure titanium. Acta Mat 60, 3849-3860.

Huang, H.W., Wand, Z.B., Lu, J., Lu, K. 2015. Fatigue behaviors of AISI 316L stainless steel with a gradient nanostructured surface layer. Acta Materialia 87, 150-160.

Hussain, A., Hao, L., Yan, C., Everson, R., 2013. Finite element simulation of the temperature and stress fields in single layers built without-support in selective laser melting. Mat Design 52, 638-647.

Leutenecker-Twelsiek, B., Klahn, C., Meboldt, M., 2016. Considering part orientation in design for additive manufacturing. Procedia CIPR 50, 408-413.

Mohr, G., Altenburg, S.J., Hilgenberg, K., 2020. Effects of inter layer time and build height on resulting properties of 316Lstainless steel processed by laser powder bed fusion. Additive Manufacturing 32.

Molaei, R., Fatemi, A., 2019. Crack paths in additive manufactured materials subjected to multiaxial cyclic loads including surface roughness, HIP, and notch effects. Int J Fatigue 124, 558-570.

Pickard, A., Knott, J., 1988. Effects of Testing Method on Cyclic Hardening Behavior in Face-Centered-Cubic Alloys. In: Solomon, H., Halford, G., Kaisand, L., Leis, B. (eds). Low Cycle Fatigue, 58-76.

Polák, J., Klesnil, M., Lukás, P., 1977. On the cyclic stress-strain curve evaluation in low cycle fatigue. Mater. Sci Eng. 28, 109-117.

Ronneberg, T., Davies, C.M., Hooper, P.A., 2020. Revealing relationships between porosity, microstructure and mechanical properties of laser powder bed fusion 316L stainless steel through heat treatment. Materials and Design 189.

Sprengel, M., Ulbricht, A., Evans, A., Kromm, A., Sommer, K., Werner, T., Kelleher, J., Bruno, G., Kannengiesser, T., 2021. Towards the optimization of post laser powder bed fusion stress relieve treatments of stainless steel 316L. Submitted to Metallurgical and Materials Transactions A.

Zerbst, U., Bruno, G., Buffiere, J.-Y., Wegener, T., Niendorf, T., Wu, T., Zhang, X., Kashaev, N., Meneghetti, G., Hrabe, N., Madia, M., Werner, T., Hilgenberg, K., Koukolíková, M., Procházka, R., Džugan, J., Möller, B., Beretta, S., Evans, A., Wagener , R., Schnabel, K., 2021. Damage tolerant design of additively manufactured metallic components subjected to cyclic loading. State-of-the-art, problems, challenges. Progress in Material Science, in print.

Zerbst, U., Madia, M., Klinger, C., Bettge, D., Murakami, Y., 2019. Defects as the root cause of fatigue failure of metallic components. Part III: Cavities, dents, corrosion pits, scratches. Engng Failure Anal 97, 759-776.

Zhang, B., Li, Y., Bai, Q., 2017. Defect formation mechanisms in selective laser melting: a review. Chin J Mech Engng 30, 515-527.